COMPUTATIONAL INTERFEROMETRIC DESCRIPTION OF NESTED FLOW FIELDS

A. George Havener, Ph.D.
Assistant Professor, Mechanical Engineering
University of Dayton, Dayton, Ohio 45469

L. A. Obergefell
Staff Researcher
Systems Research Laboratories
Dayton, OH 45431

December, 1984

Abstract

Computer graphics and theoretical descriptions of density are used to obtain computer generated flow visualizations called computational interferograms. Computational interferograms are pictorially analogous to optical interferograms, and examples showing the fringe pattern for the flow about a sharp tip cone in a supersonic air stream are presented. To ascertain the effect of unsteady behavior, local density disturbances are added to the steady state flow field. This introduces irregularities to the computational interferogram like those seen in the optical interferograms. These theoretical disturbances can be varied in geometry, density description, translated with time, and strengthened or dissipated. The accuracy of computational interferometry relies on the accuracy of the theoretical density descriptions and therefore, it provides a way of verifying existing models of flow fields, especially those containing unsteady or turbulent behavior. In addition to being a unique method of flow visualization, computational interferometry can be used to develop and modify theories or numerical solutions to both simple and complex flow fields. The present research is a general description of this process.

Keywords

Computational Interferomenty, Interferometry, Computational Flow Fields, Optical Flow Fields

Introduction

This research describes an innovative process for depicting and understanding specific details of flow fields. The process is called

computational interferometry, and it combines the drawing features of computer graphics with the principles of interferometry to obtain computer drawn displays of numerical solutions to flow fields.

Computational interferometry is a unique approach to obtaining flow field visualizations and a relatively new approach to the general study of simple and complex flows. The main ideas of this process originally Reference 3. The present work refines the original process to handle asymmetric and nested flows. The motivation for this research stems from the fundamental difficulties associated with normal interferometric applications, especially to complex flows. Normal applications are troubled by adequate treatment of the derivative of the experimental data, coping with limited data, and are generally restricted in scope to 3-D axisymmetric flows. Conceptually, computational interferometry is not effected by these problems. The present research describes a general process for treatment of asymmetric flows, and special development is made for nested flow fields. The term "nested flow" as used here pertains to central fields that are embedded with one or more smaller fields. The smaller fields of this research are ficticious, but they are representative of local turbulent structures commonly found in real in many flows.

Theoretical Modeling

Interferometry is an optical process that can be used to measure variations in optical path length. Optical path length is proportional to the density integrated along the geometric path, and therefore, interferometry can be used to measure density variations in a defined volume. Basic techniques using interferometry are well documented (Ref.1,2).

The basic equation for the interferometry process is,

$$S_i = G\int f(x,y,z)\,dl_i \qquad (1)$$

where,

$S_i(x,y)$ is the fringe shift.
G is a constant that depends on the wavelength and a reference density.
l_i is the geometric length traveled by the light waves.
$f(x,y,z)$ is the density function.

The present study is for the axisymmetric flow about a sharp tip cone, and the curvature of the light waves through the flow field is assumed to be small compared to the distance traveled by the waves. Figure 1 shows the coordinates and line of sight for this case.

For axisymmetric fields that are assumed to be refractionless, $S(x,y) = S(y)$ and $f(x,y,z) = f(r^2)$ where $r^2 = y^2 + z^2$. Then for any plane normal to the x-axis ($x = x_c$), Equation (1) becomes,

$$S(y) = G\int_{y^2}^{r^2} \frac{f(r^2)}{\sqrt{r^2 - y^2}}\,dr^2 \qquad (2)$$

Following the method of Bradley (Ref. 7), evaluation of Equation (2) is done using the transformations:

For which,

$$\eta = 1 - (r/R)^2; \qquad \xi = 1 - (y/R)^2 \qquad (3)$$

$$S(\xi) = GR\int_0^{\xi} \frac{f(\eta)}{\sqrt{\xi - \eta}}\,d\eta \qquad (4)$$

Equation (4) is seen to be Abels integral equation which can be evaluated when $f(\eta)$ is aptly defined. For example, if $f(\eta)$ is represented by a polynomial, all integrals are finite at both limits even though the integrand is singular at $\eta = \xi$.

For experimental applications, the unknown quantity is $f(\eta)$, the

density, which is sought from a knowledge of $S(\xi)$, the fringe shift. Mathematically, $f(\eta)$ is obtained by inverting Equation (4), a step that has two general difficulties. First, unless the flow field is two dimensional or 3-D axisymmetric the inversion can not be done because there is no general analytical solution to Equation (3) for asymmetric fields. Second, inversion of Equation (3) requires differentiation of $S(\xi)$. Since $S(\xi)$ is based on experimental measurements, differentiation can easily amplify scatter in the $S(\xi)$ data to a level where the final determination of $f(\eta)$ is worthless.

The Computational Interferometric Approach

Computational interferometry is a reverse of the experimental approach. Starting with a known $f(\eta)$, Equation (4) is used to calculate $S(\xi)$ for the entire field. Then, computer graphics are used to draw the $S(\xi)$ data, and the final result is a computer generated interferogram that is similar to the corresponding real interferogram. Note that since the computational interferogram results from direct application of Equation (4), no inversion is required, no differentiation of data is done, and the flow fields may be complex or asymmetric. Conceptually, only a proper description of $f(\eta)$ and Equation (4) are required. In the present application, the density throughout the inviscid flow is known from the Taylor-Maccoll solution for a cone (Ref. 8) whereas the density in the boundary layer is determined from a numerical solution for axisymmetric boundary layer flow (Ref. 5).

A fringe in an interferogram is a line of constant optical phase. The spacing between adjacent fringes defines one wave length changes in the optical path lengths through the field. When an interferometer is

adjusted to produce a finite fringe interferogram in which the reference fringes are oriented vertically, an optical reference field of known phase is established. Along any fringe, the phase is constant which means the optical path lengths are also constant. When local changes in the optical path lengths are introduced, the optical phase of the waves changes which results in a lateral bending of the fringes from their vertical orientations. The bending is necessary to maintain the continuity of the preestablished phase relationships, and the magnitude of the bends--the fringe shifts--is directly proportional to the local changes in the optical path lengths through the field.

Figure 2 illustrates the fringe shift principles for an interferogram of the cone case. Only two fringes and the upper plane are shown to simplify the diagram. As shown, the local coordinates of fringe 1 are (x,y) which are defined with respect to the body axis system located at the tip of the cone. The x_c plane is taken to coincide with the reference position of fringe 1. Due to increases in the optical path lengths through the inviscid field, fringe 1 is bent laterally to the right, the magnitude of this shift is, $S = \ell/D$. Had the optical path lengths decreased, fringe 1 would have shifted to the left. Note that this happens for the boundary layer, because the optical path lengths through the boundary layer are less than those of the inviscid flow fields. The length, ℓ, is the actual distance that fringe 1 is shifted and D is the reference spacing between fringes 1 and 2. The distance D signifies that in the reference state, the optical path length for fringe 2 is one wave length longer than it is for fringe 1. The ratio of ℓ/D is, therefore, a percentage change in the optical

path length relative to fringe 1 and the x_c plane. Therefore, the coordinates are seen to be,

$$X = X_c + \ell = X_c + SD \; ; \quad Y = X \tan\phi \tag{5}$$

For the conical flow of the inviscid field, the fluid properties are only functions of the angle ϕ and the fluid properties are constant along rays for ϕ equal to a constant. Hence, fringe shifts can be ritten as,

$$\frac{S}{X} = \frac{S}{X_c} = \left(\frac{S}{X}\right)_{ref} \tag{6}$$

and rearranging terms, the x, y coordinates are,

$$X = \frac{X_c}{1-(S/X)_{ref} D} \qquad Y = \left(\frac{Y}{X}\right)_{ref} X \tag{7}$$

The quantity $(S/x)_{ref}$ is obtained by numerically evaluating Equation (4) for a reference x_c plane and subsequently dividing each computed S by x_c. To obtain a polynomial function for the density discrete values of density are calculated from a numerical solution to the Taylor-Maccoll differential cone equation for covical flow. Then the radial distribution of density is obtained from a least squares curve fit of these computed Taylor-Maccoll values. The distribution of density in planes normal to the cone axis is required, because the evaluation of the integrals of Equation (4) is for vertical planes. Note that since Equation (4) is defined in terms of the transformed coordinates, the polynomial distribution for the density must be expressed in terms of η. Substituting the polynomial into Equation (4) and completing a term-by-term evaluation of the integrals,

$$S(\xi) = 2GR\sqrt{\xi}\sum_{i=0}^{m}(i)!\,b_i\,\xi^i\left(\sum_{j=0}^{i}\frac{(-1)^j}{(2j+1)(j)!\,(i-j)!}\right) \qquad (8)$$

Evaluation of the interferometric integral involves a double series; one series accounts for the polynomial distribution of the density while the other series is a consequence of the term-by-term evaluation of the integral. The accuracy of this fringe shift computation for the inviscid flow is discussed in Ref. 4 where the relative error is shown to be less than 0.15%.

With fringe shift data now available, the procedure for computing the coordinates of the fringes for the inviscid field is:

(1) Select D, the reference fringe spacing.

(2) Select x_c, the fringe starting position.

(3) Compute from $\phi = \tan(y/x_c)$ for each y coordinate where $(S/x)_{ref}$ is known.

(4) Compute (x,y) from Equation (7) for all values of $(S/x)_{ref}$.

(5) Index x_c by D; $x_c = x_c + D$.

(6) Repeat steps (2)-(5) until the field is defined completely.

For the boundary layer, the fluid properties are not constant along rays eminating from the cone tip, nor are they scalar multiples from one plane to the next. Consequently, a new radial distribution for the density is required for each new x plane being surveyed. This leads to an iteration process. The quantities required are the boundary layer thickness and the radial distribution for the density. Both of these are obtained from theory (Ref. 5). The iteration procedure involves picking x and y and using Equation (8) with additional terms for the boundary layer to compute S. This value is compared to $S = \ell/D$, and x is iterated until the two S values agree.

Figure 3 is a computational interferogram that illustrates the

above procedures. The field is for supersonic flow over a sharp tip cone and includes treatment of the boundary layer. The straight fringes of the reference region are seen to shift abruptly to the right as they cross the shock wave. Then they make a smooth curve through the inviscid field to the boundary layer at which point they shift back to the left. The fringe reversal in the boundary layer is due to a shortening of the optical path lengths for this region.

Computational Interferometry for Nested Flow Fields

The fringes seen in interferograms of real flow fields are generally unlike the smooth, uniform fringes of the computational interferograms, because the real flow fields often contain time varying local disturbances that are omitted from the theoretical solutions. For example, real flow fields can contain turbulent eddies which are seen as irregularities in the interferograms. Figure 4 exhibits an irregularity which is circled for identity. This is an enlargement of a section of the flow field presented in Figure 6. The exact nature of the irregularity is unknown, and because only one view of this flow field is possible, an exact determination of the density associated with this irregularity can not be determined from this interferogram. Since this irregularity is in the midst of a presumeably stable field, the interferogram definitely shows the presence of a secondary flow. Using computational interferometry, a possible resolve of this irregularity--the others as well--is obtained by inserting secondary flow fields in the theoretical description of the primary field, and then by computing and displaying the resultant alterations to the fringe pattern.

When secondary flows are placed in the primary flow, the composite field is no longer axisymmetric, and Equation (8) must be changed. The integration is still valid for y = constant, but $f(\eta)$ must be modified to account for the secondary fields.

An illustrative example of an embedded field is shown in Figure 5. The primary field is still the inviscid field, and it is centered on the y-z axes. The disturbance is arbitrarily located a distance h and k from the y-z axes respectively.

The principle of linear superposition is used to determine the fringe shift for the y_i ray passing through this composite field,

$$S(y_i) = S_i(y_i) + S_d(y_i) \tag{9}$$

Here, $S_i(y_i)$ is the fringe shift for the inviscid field and $S_d(y_i)$ is the fringe shift for the embedded disturbance. $S_i(y_i)$ is expressed as the fringe shift of the disturbance free field minus the portion occupied by the disturbance,

$$S_i(y_i) = G\int_{y^2}^{R^2} \frac{f(r^2)}{\sqrt{r^2 - y^2}}\, dr^2 - S_{id}(y_i) \tag{10}$$

where $S_{id}(y_i)$ is the inviscid field contribution to the total fringe shift that is overlapped by the disturbance. $S_{id}(y_i)$ is determined using Equation (1) and integrating from z_1 to z_2.

$$S_{id}(y_i) = G\int_{z_1}^{z_2} f(y_i, z)\, dz \tag{11}$$

Since the inviscid field is axisymmetric,

$$S_{id}(y_i) = \frac{G}{2}\int_{r_1^2}^{r_2^2} \frac{f_i(r^2)}{\sqrt{r^2 - y_i^2}}\, dr^2 \tag{12}$$

From the circular geometry of the disturbance,

$$r_1^2 = z_1^2 + y_i^2 = \left[h - \sqrt{\gamma - (y-k)^2}\right]^2 + y_i^2$$

$$r_2^2 = z_2^2 + y_2^2 = \left[h + \sqrt{\gamma - (y-k)^2}\right]^2 + y_i^2 \qquad (13)$$

Using Bradley's transformations,

$$g_1(\xi) = 1 - \left(\frac{r}{R}\right)^2 \qquad g_2(\xi) = 1 - \left(\frac{r}{R}\right)^2$$

Equation (12) becomes,

$$S_{id} = GR \int_{g_1(\xi)}^{g_2(\xi)} \frac{f_i(\eta)}{\sqrt{\xi - \eta}}\, d\eta \qquad (14)$$

Equation (14) is solved in the same manner as the axisymmetric case, and $f_i(\eta)$ is the same density function as that used in Equation (3).

For the disturbance $S_d(y_i)$ is,

$$S_d(y_i) = G \int_{Z_1}^{Z_2} f_d(z)\, dz \qquad (15)$$

$f_d(z)$ is the density function for the disturbance at (x_c, y_i).

To avoid a discontinuity at the geometric boundaries of the disturbance, $f_d(z)$ is matched with $f_i(z)$ at z_1 and z_2, and a peak density is arbitrarily chosen for the center point. With these three points known, a quadratic distribution for the density as a function of z is calculated and used to evaluate Equation (15).

The computational interferogram for the nested fields is obtained in the same manner as the interferogram for the axisymmetric field, but when a light ray falls within the disturbance boundaries, a combined fringe shift is calculated using Equations (8), (14) and (15). This calculation is a trial and error process in which an interation for the x coordinate of the fringe is carried out for a constant y coordinate. The process involves selection of x, calculation of S(y) using Equations (5), (8) and (9), and a second calculation of S using $S = \ell/D$. The two S values are compared, and the intersection process is repeated until

these S-values agree. Computational interferograms for multiple disturbances are obtained in a similar manner simply by summing the contribution of each disturbance.

Results

Figure 6 shows a comparison between the computational and optical interferograms for a flow field similar to that of Fig. 3. This flow field is for steady state, irrotational, adiabatic, inviscid flow with a boundary layer over a sharp tip cone in a supersonic air stream. The agreement between these two interferograms is good but there are some differences. The main difference between the two interferograms of Fig. 6 is the nonuniformities and subtle irregularities in the fringes of the optical interferogram. These irregularities are present because the optical interferogram is an instantaneous recording of an unsteady turbulent flow field and these irregularities are exhibiting the turbulence. For the present research, models for these disturbances are added to the computational interferogram by nesting ficticious density fields in the inviscid field. The disturbance fields selected here are arbitrary and are used only to study the disturbance effects on the fringe pattern and the general degradation of the fringe patterns in interferograms of stable, steady flows.

A computational interferogram for a section of the inviscid field is illustrated in Fig. 7. This section is a nested field because it contains a disturbance. The geometric description of this disturbance is a diamond that has circular cross sections. The density of every point on the boundary of the disturbance is matched with the corresponding inviscid field density at all respective boundary points.

Comparing Figures 4 and 7, the computational fringe distortions of Figure 7 are beginning to resemble the irregularities seen in real interferograms. This strongly suggests that more careful and realistic modeling of the disturbances would produce good agreement between the computational and optical interferograms.

A final result of the present research is presented in Fig. 8. Figure 8 is a computational interferogram for a flow field with two nested disturbances. The disturbances are equal in geometry and they have the same centerline density distributions. However, as seen in Fig. 8, these disturbances have distinctly different effects on the fringe pattern. The upper disturbance is the same as that of Fig. 7. It is located in the primary field along the y-axis (h = 0, Figure 5). The lower disturbance is located off both axes. This disturbance occupies a portion of the primary field where the density of the primary field is stronger than that of the position of the upper disturbance. Hence, there is a net reduction in the optical path lengths for this disturbance which causes the fringes to bend to the left. The results of Fig. 8 are significant, because they show clearly that not only are the geometric definitions and the continuity of density distributions important factors, but the location of the disturbances within the field are of equal concern.

Conclusions

Computational interferometry is an innovative technique that can be used to obtain flow visualizations of theoretical flow fields. These interferograms are in every way analogous to the optical interferograms

of real flow fields, because they describe the theoretical phase content of events in the same way as the real interferograms. Practical application of computational interferometry lies in its usefulness to exhibit the numerical solution of flow fields in a way that allows researchers the opportunity to see the event just as it would appear in reality. A significant extension of computational interferometry involves applications to the analysis of nested flow fields, transient events and unsteady behavior in a manner that permits direct comparision to real flows. While the disturbance models studied in this research are ficticious, the effects they produce on the central fringe pattern indicate that with proper fluid dynamic modeling, the interferometric structure of flow field disturbances can be drawn and studied in detail. This capability is not known to exist in any other flow visualization process.

The most serious limitation of computational interferometry appears to be the concern for uniqueness: Can more than one arrangement of disturbances produce identical interferograms? The scope of this research can not answer this important question, and it certainly seems that more than one arrangement of nested flows could produce identical interferograms. Remembering that these nested fields are not axisymmetric and that more than one view of an asymmetric field is required for a complete analysis, the answer of uniqueness lies in drawing multiple views of computational interferometry for the same event, and then comparing these interferograms to optical interferograms of the real event. Accomplishing the latter step is difficult, possibly even impossible for transiant events, because multiple views of real flow fields are very difficult to obtain.

Recommendations

The findings of this research definitely suggest additional study. First, development for real disturbances should be undertaken so that more meaningful comparisons to optical interferograms of real events can be done. Following this, the question of uniqueness should be resolved by conducting a comprehensive experimental and theoretical study of a reproduceable asymmetric nested flow field which leads itself to multiple viewing.

Acknowledgements

Acknowledgement is given to the Computational Aerodynamics Group, Aeromechanics Division, Air Force Flight Dynamics Laboratory, AFWAL, WPAFB, Ohio for use of their computing facilities.

References

1. Vest, C.M., Holographic Interferometry, John Wiley and Sons, New York, 1979.
2. Havener, A.G., "Users Guide Pulse Laser Holography For Wind Tunnel Testing," Aerospace Research Laboratories, ARL TR-0123, AD/A017710, June, 1975.
3. Havener, A.G., Grove,J., Hankey,W., "The Application of Computer Graphics Techniques to the Interferometric Description of Supersonic Flow About a Sharp Tip Cone at Zero Angle of Attack," AFFDL TM 79-15-FXM, (FOR OFFICIAL USE ONLY), Wright Patterson Air Force Base, Ohio, Nov. 1978.
4. Havener, A.G., "On the Application of Holographic Interferometry to Axisymmetric Air Flows," Ph.D. Dissertation, University of Dayton, Dayton, Ohio, 1983.
5. Shang, J.S. and Hankey, W.L., Jr., "Numerical Solution for Supersonic Turbulent Flow Over A Compression Ramp," AIAA Journal, Volume 13, October 1975, pp. 1368-1374.
6. Hodge, J.K., et al. "Numerical Solution for Airfoils Near Stall In Optimized Boundary Fitted Curvilinear Coordinates." AIAA Journal, 1978.
7. Bradley, J.W., "Density Determination From Axisymmetric Interferograms," AIAA Journal, Volume 6, No. 6, June 1968, pp. 1190-1192.
8. Shapiro, A. H., The Dynamics and Thermodynamics of Compressible Fluid Flow, The Ronald Press Company, New York, 1954.

FIGURE LEGENDS

FIG. 1 Geometry and Coordinates for a Shart Tip Cone in Supersonic Flow

FIG. 2 Friner Shift Description for a Sharp Tip Cone

FIG. 3 Computation Interferogram for Inviscio Field and Boundary Layer

FIG. 4 Optical Interferogram of Fringer Irregularities

FIG. 5 Coordinates for Disturbance Location

FIG. 6 Direct Comparison Between Computational and Optical Interferograms

FIG. 7 Computational Interferogram of Disturbance with Density and Geometrical Continuity

FIG. 8 Multiple Disturbances in a Computational Interferogram

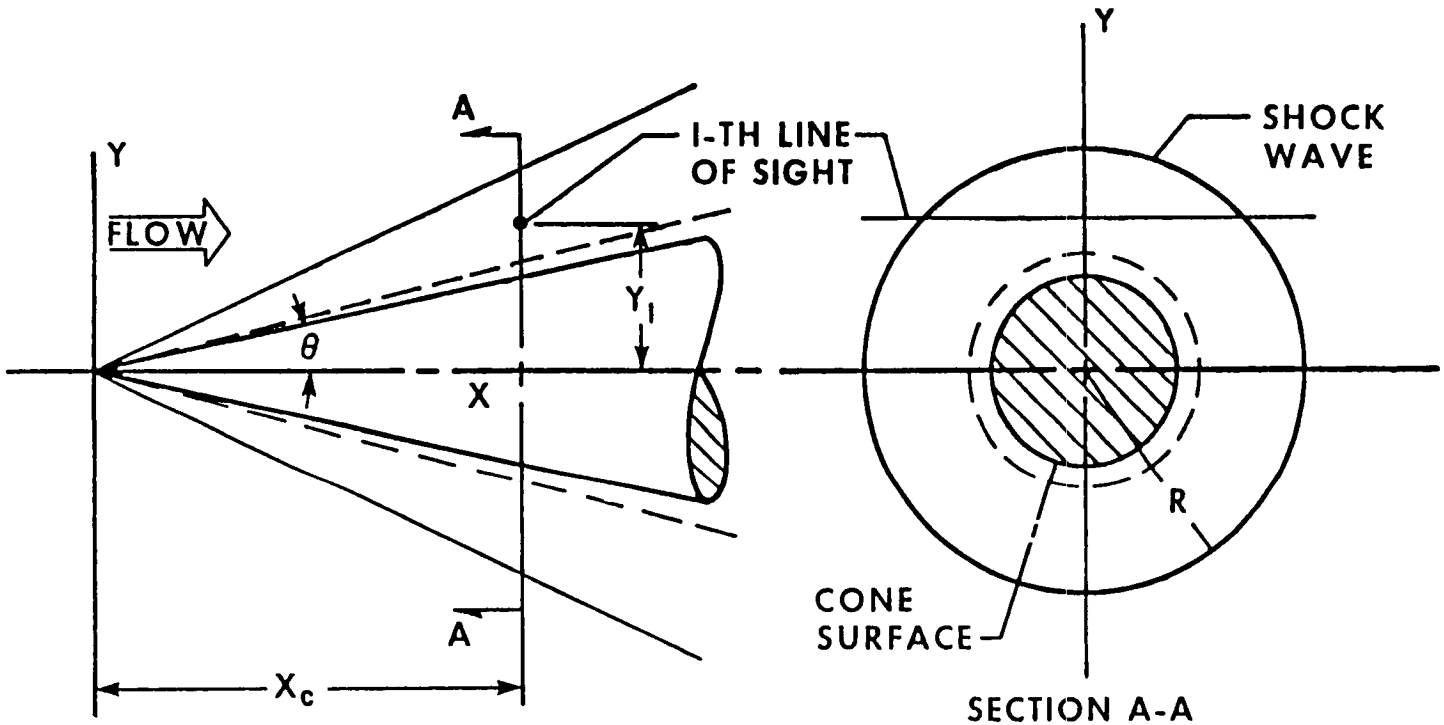
Y
FLOW
A
I-TH LINE
OF SIGHT
θ
X
Y_I
A
X_c
Y
SHOCK
WAVE
R
CONE
SURFACE
SECTION A-A

Fig. 1

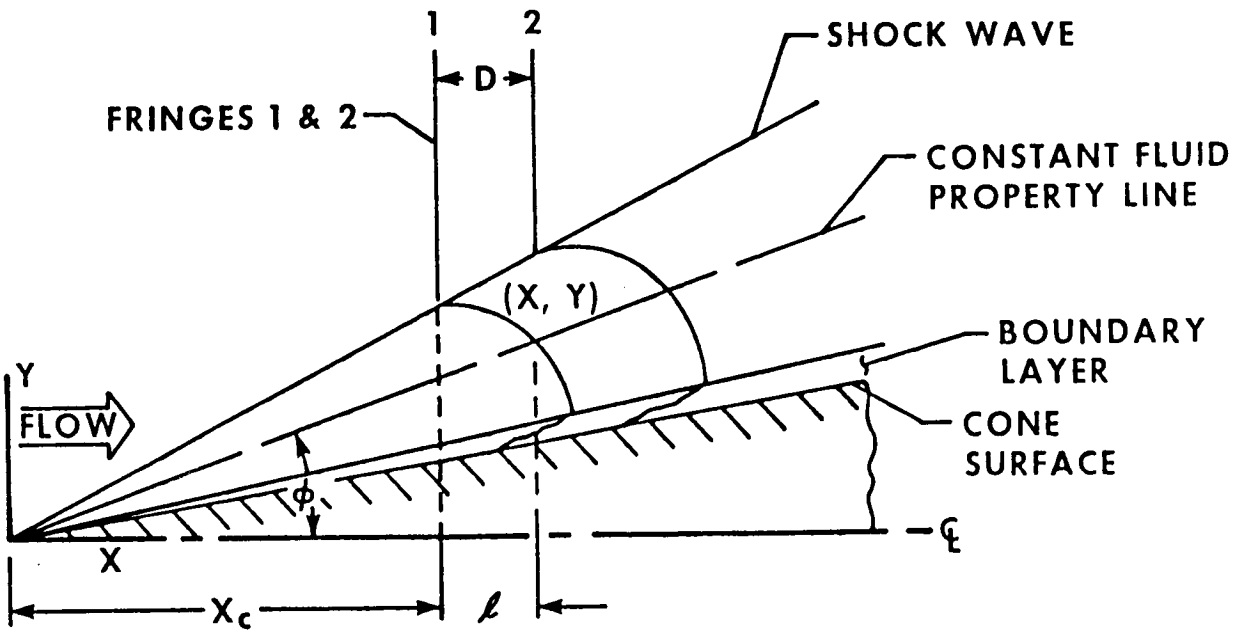
1
2
D
FRINGES 1 & 2
SHOCK WAVE
CONSTANT FLUID
PROPERTY LINE
(X, Y)
BOUNDARY
LAYER
Y
FLOW
CONE
SURFACE
ϕ
X
X_c
ℓ

Fig. 2

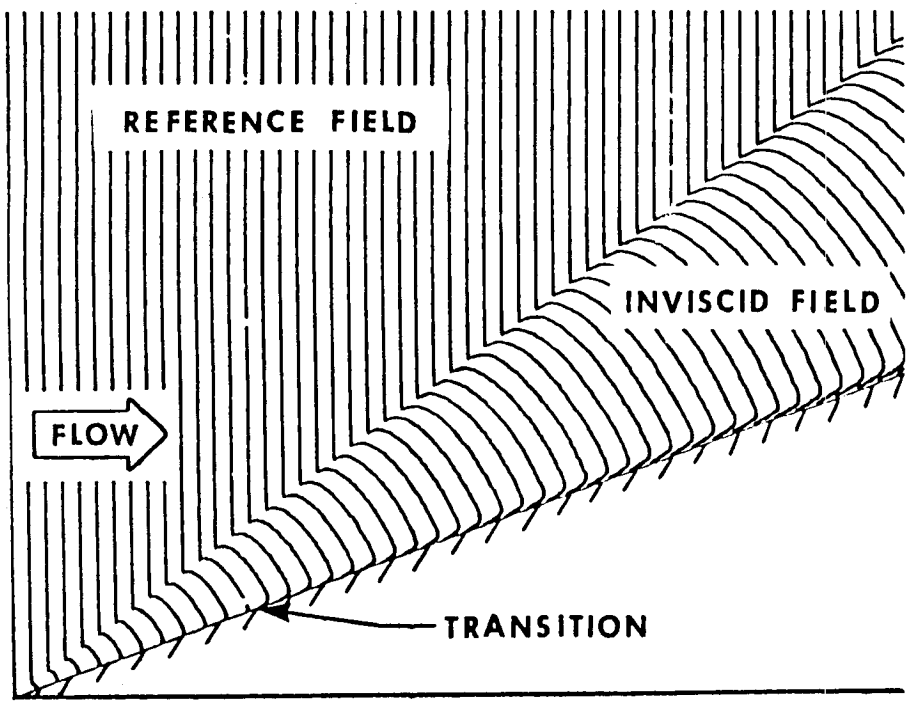

Fig. 3

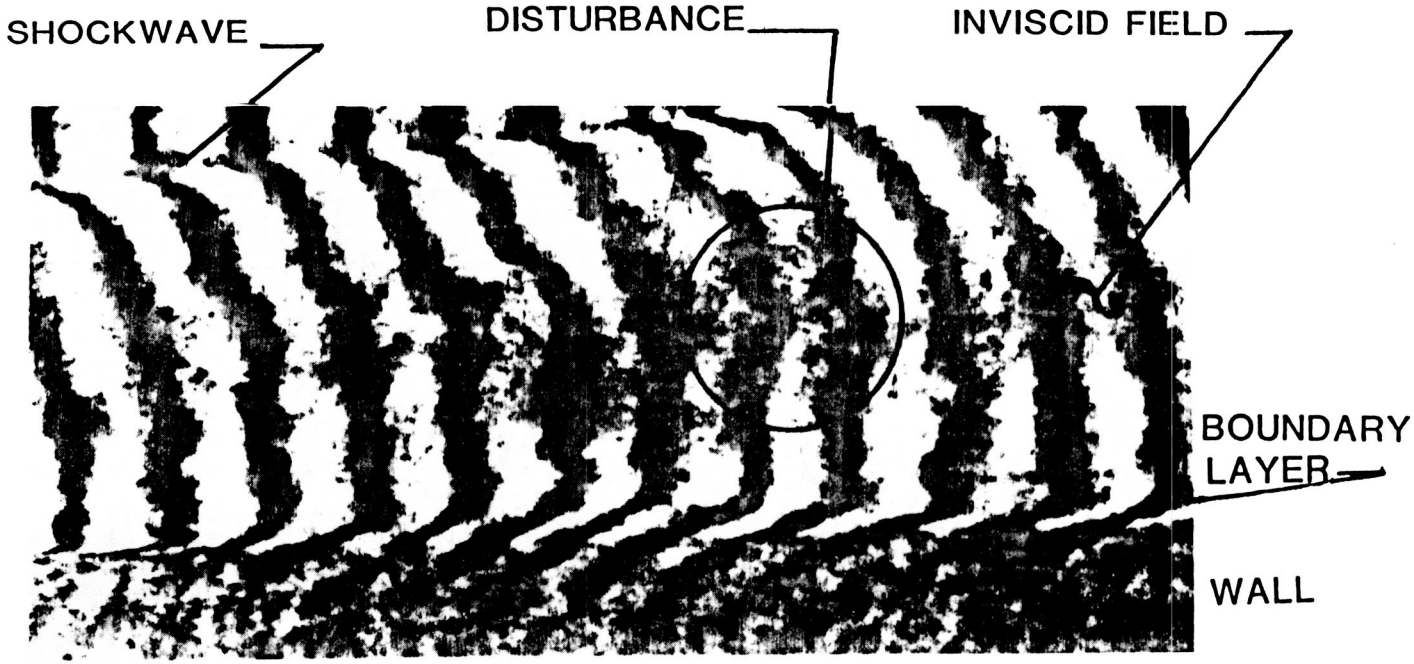

Fig. 4

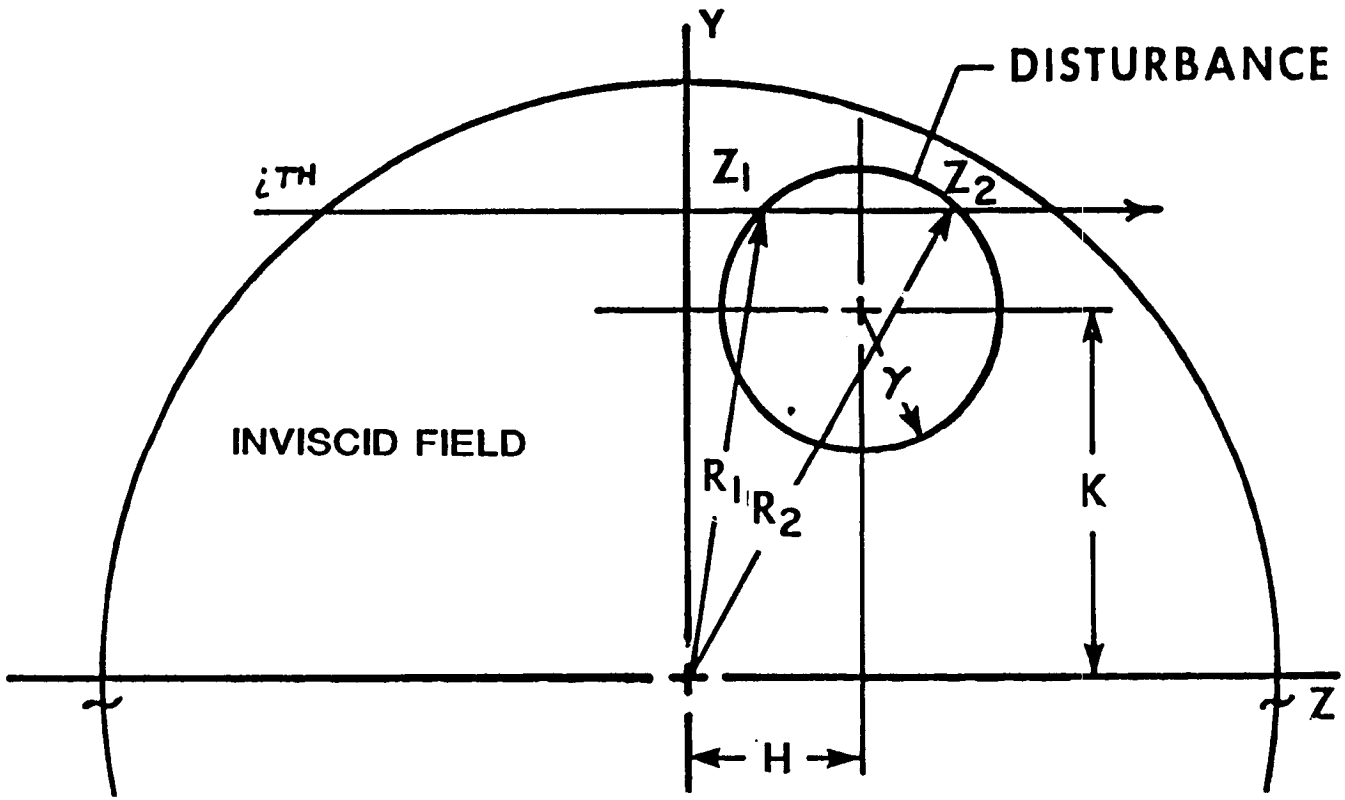

Fig. 5

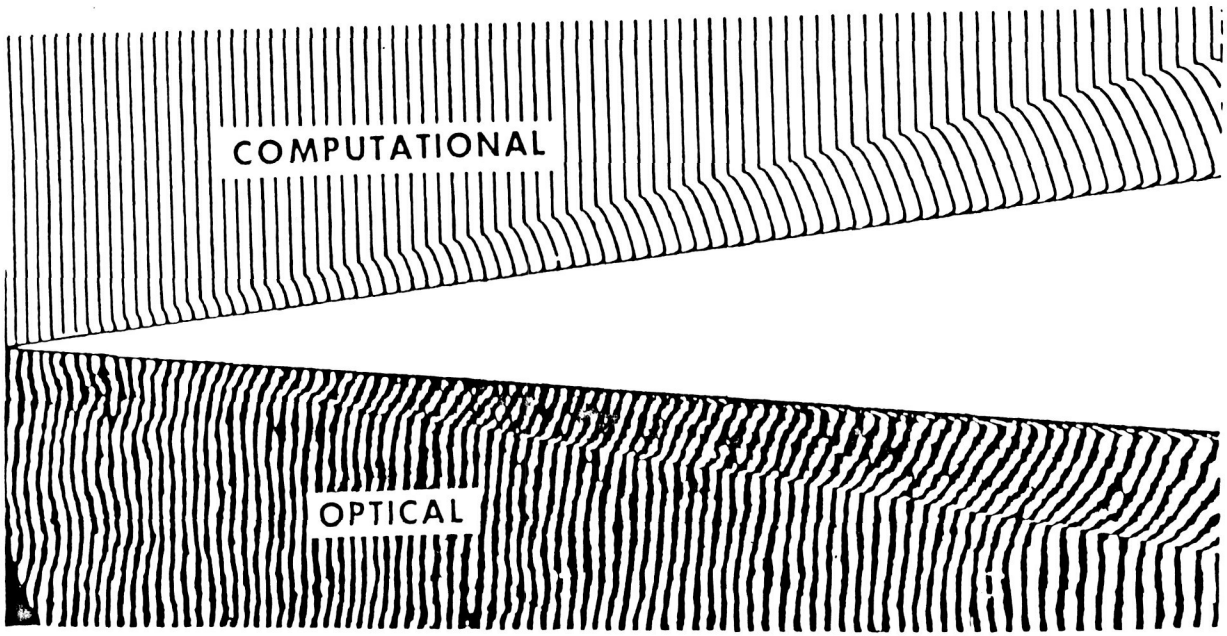

Fig. 6

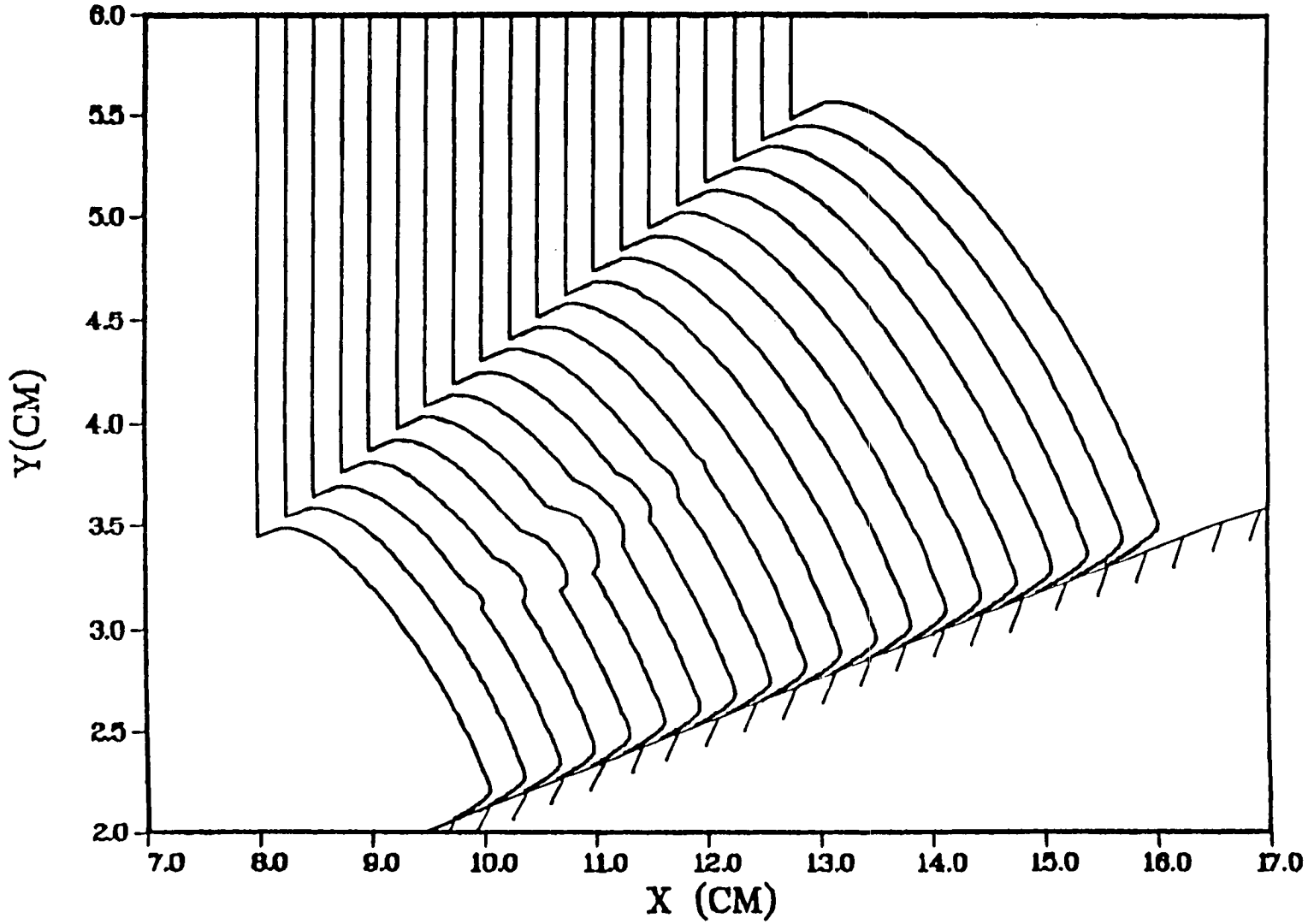
6.0
5.5
5.0
4.5
4.0
3.5
3.0
2.5
2.0
Y(CM)
7.0
8.0
9.0
10.0
11.0
12.0
13.0
14.0
15.0
16.0
17.0
X (CM)

Fig. 7.

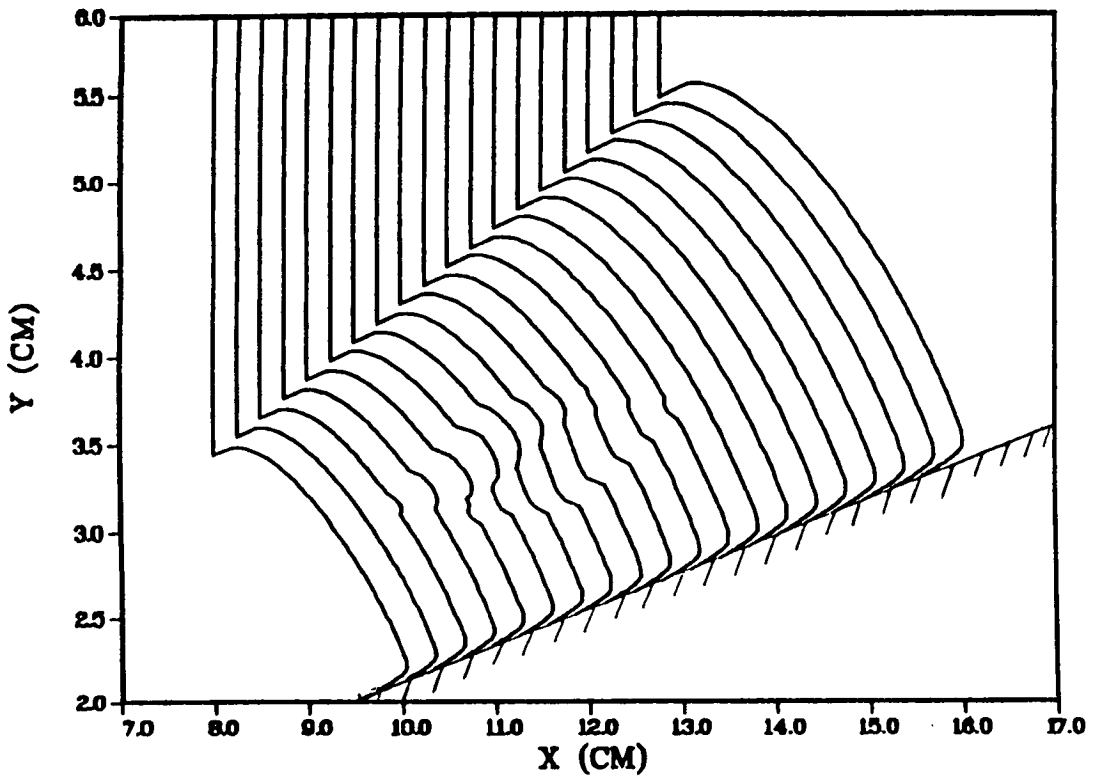
6.0
5.5
5.0
4.5
4.0
3.5
3.0
2.5
2.0
Y (CM)
7.0
8.0
9.0
10.0
11.0
12.0
13.0
14.0
15.0
16.0
17.0
X (CM)

Fig.8